Experimental investigations of welding induced temperature gradients and distortions in a segment of an OSD

Maarleveld, Arvid; Malschaert, David; Veljkovic, Milan

Publication date
2022

Document Version
Final published version

Published in
IABSE Symposium Prague, 2022

IABSE Symposium Prague 2022
Challenges for Existing and Oncoming Structures
May 25-27 2022, Prague, Czech Republic

Experimental investigations of welding induced temperature gradients and distortions in a segment of an OSD

Arvid Maarleveld, David Malschaert, Milan Veljkovic

Faculty of Civil Engineering and Geosciences, Delft University of Technology, 2628CN, Delft, the Netherlands

Contact: a.maarleveld@student.tudelft.nl

Abstract

Orthotropic bridge decks are susceptible to fatigue cracks which are influenced by the thickness of their components, welding procedure, type of the weld, the position of the considered detail in relation to the local loading condition and by residual stresses due to welding. The above-mentioned parameters determine the detail category for fatigue resistance. This research focuses on an experimental investigation of the temperature distribution and distortions due to the welding of a connection between the deck plate, longitudinal stiffener and crossbeam. Three specimens were welded with dimensions of: 900x400 mm deck plate, 350mm deep trapezoidal longitudinal stiffener and 600mm long crossbeam in a workshop of a bridge fabricator. The crossbeams were manufactured with Haibach cope holes. The thickness of the deck plate and crossbeam was 15 mm, and the thickness of the longitudinal stiffener was 8mm. During the welding, the temperature was measured using a FLIR© E96 camera. The distortions were measured using an Artec Leo© scanner by comparing the initial state and the state after welding. 1.8 seconds after welding, steep temperature gradients were measured with a maximum of 1042°C. After cooling, a maximum upward displacement of 1.3 mm of the deck plate was measured. The main motivation of the experiments performed is to create a database for validation of a numerical model for the fatigue life prediction, which is left out of the scope of this paper. The order of magnitude of the deformation field is comparable to experiments found in the literature, although the results cannot be directly compared due to geometry, welding, and material differences.

Keywords: residual stresses; welding; distortions; OBD; fatigue

1 Introduction

Due to their relatively high stiffness and low self-weight, orthotropic bridge decks (OBD) have been widely used in movable and long-span bridges [1]. An OBD consists of a deck plate, longitudinal stiffeners (rib), crossbeams and main girders, as shown in Figure 2. Despite its advantages, the manufacturing process may lead to distortions and imperfections [2,3]. Furthermore, fatigue cracks have been observed in the welded connections in various bridges [4]. In Figure 2 and 3, examples are shown of cracks that have been detected in the rib-to-deck and the rib-to-crossbeam connection, including a Haibach cope hole. These cracks can be formed in locations of high-stress concentration and/or local defects and are influenced by residual stresses [5,6].

Welding induced residual stresses can reach the yield stress and are formed by steep temperature gradients and the restrained thermal shrinkage during the cooling [6,7]. Residual stresses have a large influence on fatigue life and therefore

knowledge of the distribution is required for accurate fatigue assessment [8]. Several experimental, as well as numerical methods have been established to determine residual stresses. The incremental hole-drilling method is popular due to its ease of use. It was used by many researchers including van Puymbroeck et. al [9] and Gu et al. [10]. In the latter research, results were compared to a finite-element model based on a subsequently coupled thermo-mechanical finite-element model where the heat source was substituted by the Goldak [11] double ellipsoid heat source model (DEHSM). Deviations between experimental and numerical results were within 20 MPa. Distortions have also been measured in recent research. This knowledge is required to take appropriate distortion control measures and to derive residual stresses from the deformation field. Deng et al. [2] measured distortions of a thin plated specimen by tracking coordinates of targets with a 3D photography technique, while Sim et al. [1] measured distortions in full-scale bridge deck specimens with a laser tracking system.

The residual stress distribution depends on many factors including welding parameters, welding speed, chemical composition of the steel, resultant weld geometry and weld toe radius [12]. To be able to gain confidence in reducing the complexity of finite element models by applying simplifications and/or assumptions, validation with experimental research is required.

This research aims to establish an experimental methodology and a database of temperature gradients and distortions in a segment of an OBD. Thermal measurements are performed by a FLIR E96 thermal camera. Distortions are derived from 3D geometry scans by use of an Artec Leo scanner.

Firstly, the specimen characteristics and experimental set-up are discussed followed by the methodology. Finally, thermal- and distortion results are presented.

2 Methodology

2.1 Specimen characteristics

Three specimens have been manufactured with dimensions shown in Figure 4. Each specimen was made out of S355J2+N. The specimens were welded by gas metal arc welding (GMAW). The shielding gas consisted 80% out of Argon and 20% out of CO2. The gas flow rate was between 15 and 20 L/min. The used filler wire type was Diamondspark 52RC (1.2 mm) for the vertical passes and MC715H (1.2mm) for all other passes.

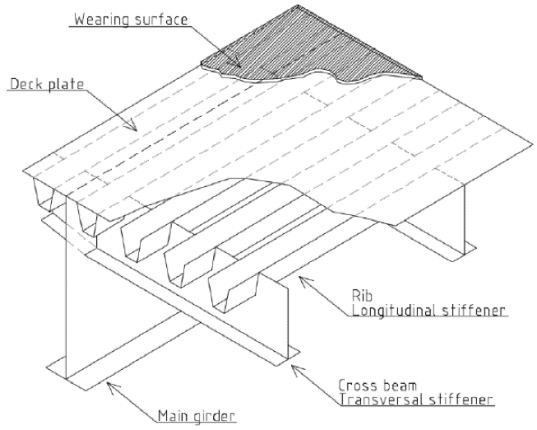

Figure 1. Orthotropic steel deck overview [13]

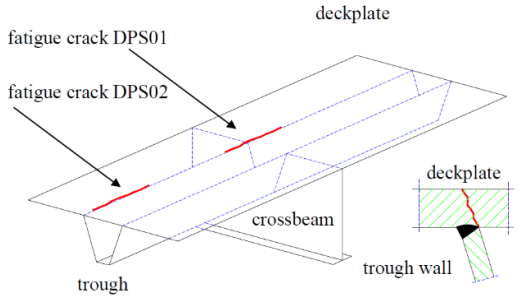

Figure 2. Crack in the rib-to-deck connection [4]

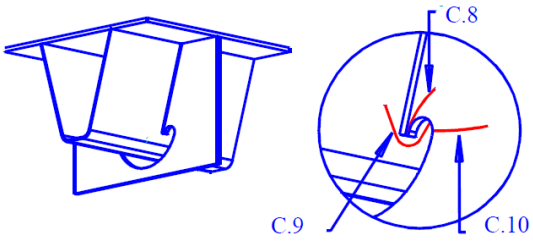

Figure 3. Crack in the rib-crossbeam connection with cope hole [4]

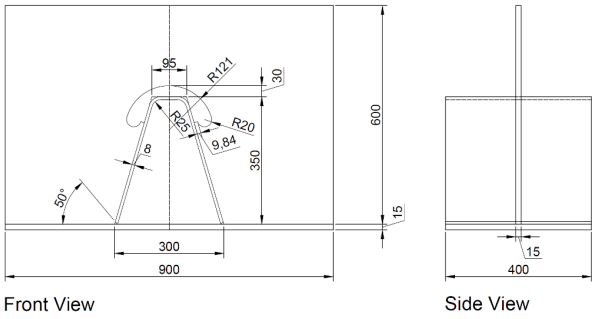

Figure 4. Specimen dimensions

2.2 Experimental set-up and measuring equipment

The experimental set-up is shown in Figure 5. The temperatures were measured using a thermosensitive FLIR E96 camera which was placed on a tripod during the welding of specimens. Radiometric video was recorded at 30 fps with a resolution of 640x480 pixels. During welding, the sensor was covered to protect it from the high radiation emitted by the welding torch. After welding, the sensor was uncovered to measure the temperature directly after welding. The accuracy of the measurements is ± 2°C or ± 2% [14]. Three temperature ranges could be selected, -20°C to 120°C, 0°C to 600°C and 300°C to 1500°C. The temperature ranges of 0-600°C and 300-1500°C were used during the experiment to capture the entire temperature scale. For distortion measurements, an Artec LEO 3D scanner was used. The Artec Leo scanner captures 3 million data points per second with an accuracy of up to 0.1mm. Frames are reconstructed from these points, from which a 3D model is made. The HD scanning algorithm was enabled, which uses more polygons per frame for data processing, leading to denser and higher quality 3D data. A 3D resolution of up to 0.2mm can be achieved with this mode. In the scanner settings, HD mode was enabled and set to 1/8, meaning that for every 8 frames, one frame was reconstructed in HD mode [15]. By comparing scans before and after welding, distortions will be obtained.

Figure 5. Experimental set-up

2.3 Experimental procedure

During the experiment, the welding- and cooling time, power input and wire feeding speed were documented. The temperature of all welding passes was recorded with the FLIR E96 thermal camera. During welding, the sides of the deck plate were constrained by welding it to the workbench to simulate neighbouring bridge deck behaviour. For representing an OBD part, these welds between the workbench and the deck plate led to over constraint. Therefore, for specimen 3, the welds of 400 mm long were removed, and the effect of these boundary conditions was investigated. The following actions have been taken during the experiment for each specimen.

1. Welding of the deck plate to the workbench.
2. Applying tack welds (see Figure 6).
3. Scanning of 3D geometry.
4. (Specimen 3) remove workbench welds of length 400 mm.
5. Weld pass 1.1-2.2 (see Figure 7).
6. Scan 3D geometry.
7. Placing of the crossbeam and tack welds (see Figure 8).
8. Scan 3D geometry.
9. Weld passes 3-10.
10. Scan 3D geometry.
11. Removing of welds connecting specimen to the workbench.

12. Scan 3D geometry.

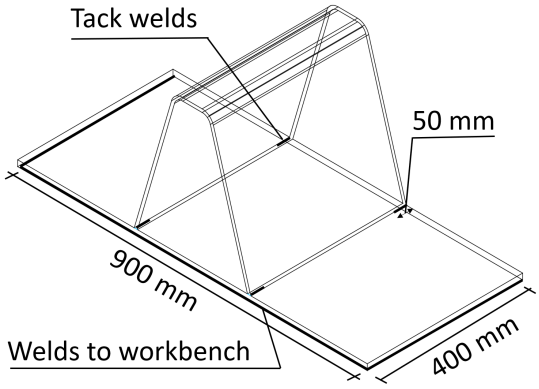

Figure 6. Location and length of tack welds before welding

2.4 Data processing

The radiometric video has been processed in FLIR research studio 2.0 software. In the software, thermal images of each frame can be exported, and the temperature range and colour palette can be changed. Various regions of interest (ROI) can also be defined, such as a point, a line, a rectangle, or a circle. Temperature values 1.8 seconds after welding along a line perpendicular and parallel to pass 1.1 have been exported, as well as a maximum temperature value in time in a box around the melting pool.

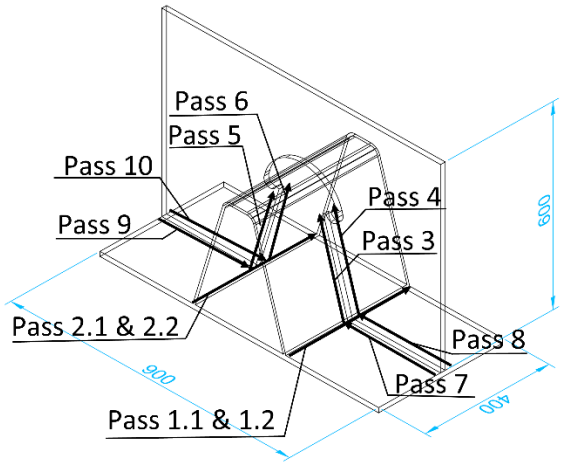

Figure 7. Welding procedure, passes

The geometry scans were post-processed in the Artec Studio 16 Professional software [15]. The post-processing steps and settings are as follows.

1. Import the scan, set HD data density to 4x.
2. Apply the global registration algorithm. This algorithm converts all one-frame surfaces into a single coordinate system.
    a. Features: Geometry and texture
    b. Search features within: 5mm
3. Apply the outlier removal algorithm. This removes 3D noise.
    a. 3D-noise-level: 3
    b. 3D resolution: 0.2mm
4. Apply sharp fusion. This fuses all frames in a single polygonal 3D model.
    a. 3D resolution: 0.2mm
    b. Fill holes with radius ≤ 5mm
5. Use the positioning tool and the transformation tool to place the coordinate system on the work bench surface, with the x-direction in the direction of pass 1.1 and the z-direction downwards.

The resulting model consisting of 74 million polygons and the location of the coordinate system is shown in Figure 9. Additional images of the weld geometry before and after welding are shown in Figures 10 and 11. Finally, the polygonal 3D model was exported to an .stl file, which contains all coordinates of the polygonal nodes in millimetres.

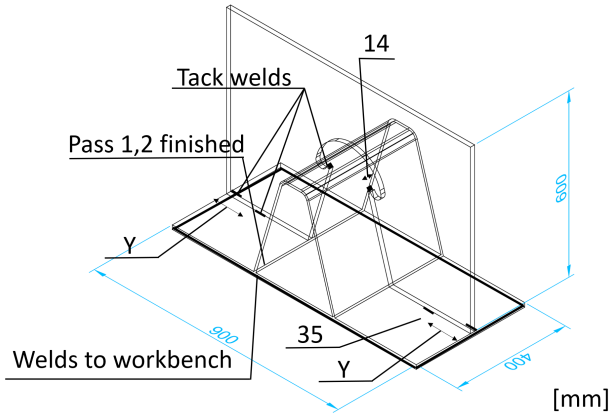

Figure 8. Tack welds after fitting the crossbeam. Distance Y is 140-180mm, depending on the specimen

With the NumPy-stl package in Python, the z-coordinates of the polygonal nodes were extracted and plotted along three paths. The paths are shown in Figure 15.

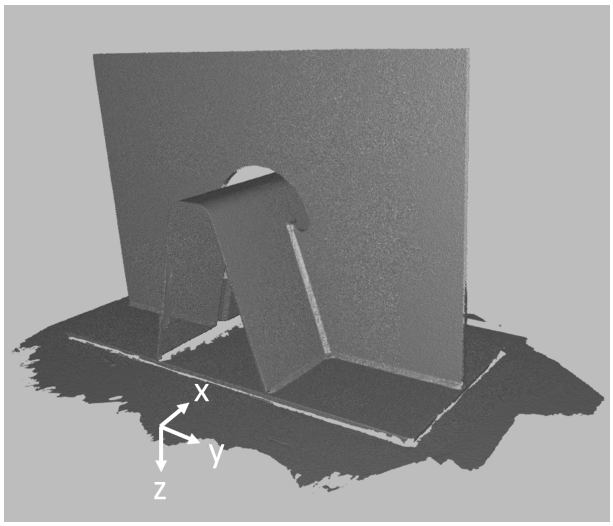

Figure 9. Polygonal 3D model in Artec studio software

This resulted in approximately 13000 points along path 1. The scattered data was filtered in Python with the Savitzky-Golay algorithm with a window size of 1999 points and a 3rd degree polynomial. The result can be found in Figure 16.

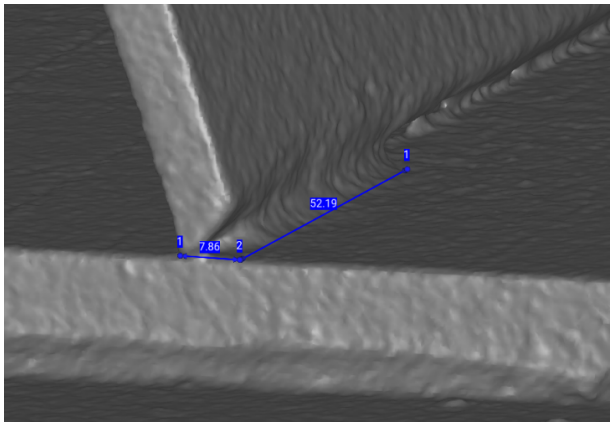

Figure 10. Tack weld geometry

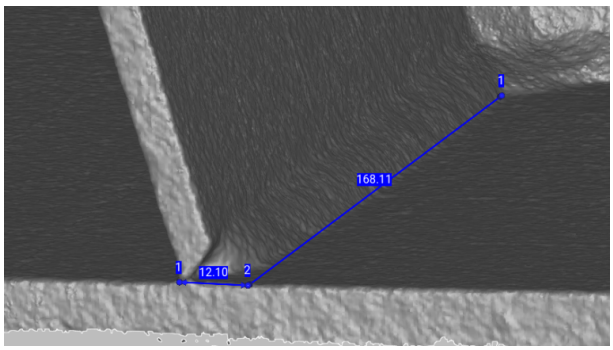

Figure 11. Final weld geometry

3 Results

3.1 Temperature

A thermal image 1.8s after the pass 1.1 in specimen 3 is shown in Figure 12. The maximum recorded temperature was 1042 °C, which is around the melting point of steel.

In Figure 13, maximum temperatures are shown at a distance x and y from the heat source, 1.8 sec after the welding. In Figure 14, the maximum temperature as a function of time in box B1 is shown. While the temperature recording range in specimen 3 was set to 300-1500C, values up to 150C were recorded. Values in specimen 3 are significantly larger at a distance of -300 to -50 mm from the heat source compared to specimen 1 in Figure 13. In specimen 1, the measured values are closer to the expected values. Both recording ranges have an accuracy of +-2%, according to the manufacturer. Focusing issues might occur in the high recording temperature range, or the specimen cools down too quickly to obtain an accurate reading in this range. This range requires special attention and a double-check with alternative equipment. However, the effect of this scattering is not expected to significantly influence the deformation (and the residual stresses).

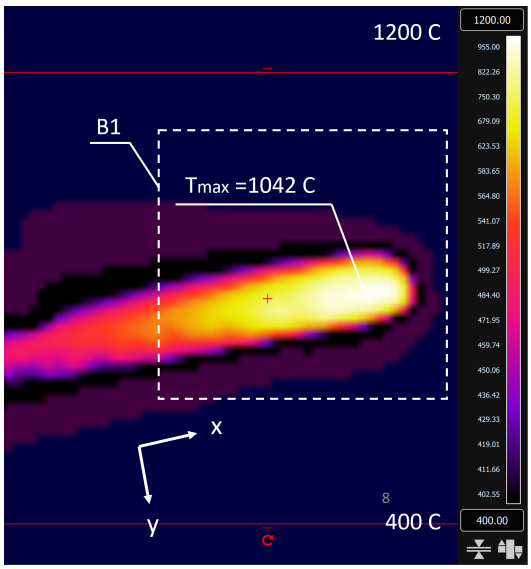

Figure 12. Thermal image specimen 3 1.8s after welding

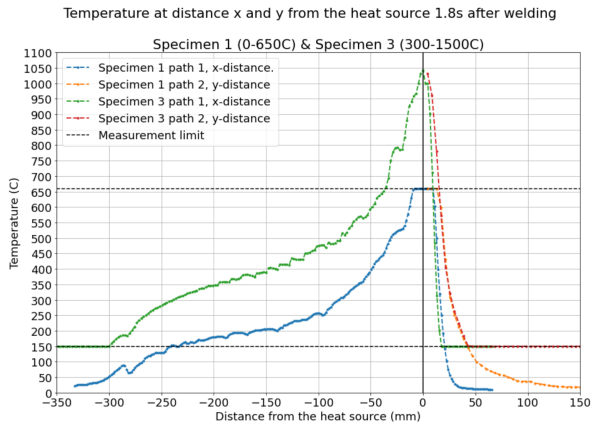

Figure 13. Temperature values at a distance x and distance y from the heat source at 1.8s after welding

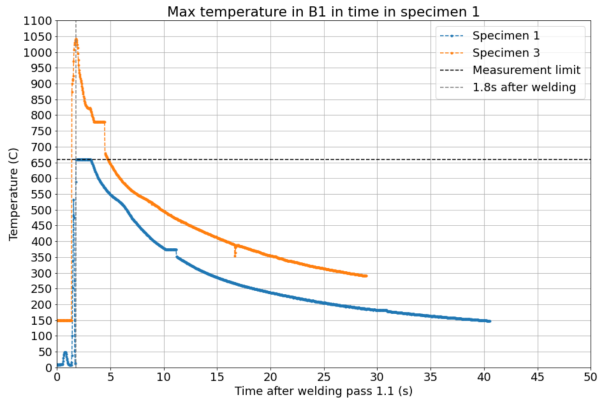

Figure 14. Maximum temperature as a function of time

3.2 Distortions

For each specimen, the z-coordinates of the polygonal nodes of the 3D model were extracted. The coordinates are plotted along paths 1,2 and 3, as defined in Figure 15. Coordinates within a range of 1mm are plotted. So, for path 1, coordinates between $x = 20$ and 21 mm from the start of the deck plate are plotted and for path 2, the coordinates are between $y = 10$ and 11 mm from the weld toe. By comparing the coordinates from the scan before welding and the scan after releasing the constraints, welding distortions are obtained.

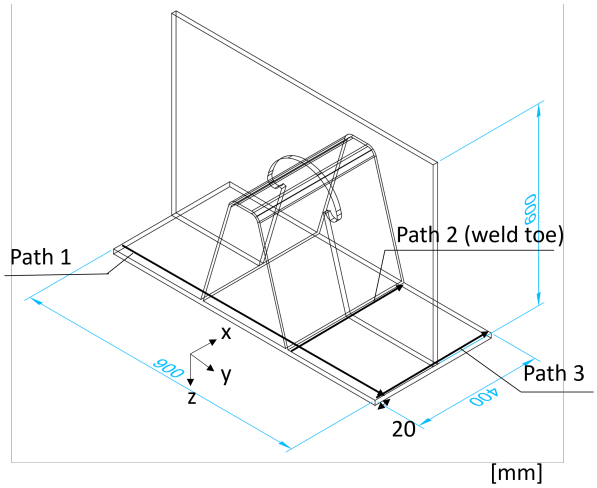

Figure 15. Paths along which z-coordinates are plotted

The resulting scattered data is filtered by the Savitzky-Golay procedure to obtain a smooth curve. The results for paths 1,2 and 3 are shown in Figures 16, 18 and 19, respectively. The top Figure shows the geometry with a large z-axis scale, while only a small scale is presented in the bottom Figure.

The largest displacement in path 1 occurs in specimen 1. Subtracting the z-coordinate after welding from the coordinate before welding at $y = -450$ mm results in an upward displacement of 1.32mm.

The order of magnitude of the deformation is comparable to deformations of the rib-deck specimens used in the research of Sim et al. [1], where four trapezoidal stiffeners without crossbeams were investigated and measures were taken at five points in transverse direction. The measured displacements are shown in Figure 17. In the research, specimen 1 was non-pre-cambered and is, therefore, the most comparable to results in this research. Upward displacements of the middle ribs are 2-3mm, compared to the initial geometry. Adding a crossbeam will reduce these values and the slope will be shallower. The values cannot directly be compared, due to the differences in geometry, welding procedure and material properties, but the order of magnitude is comparable.

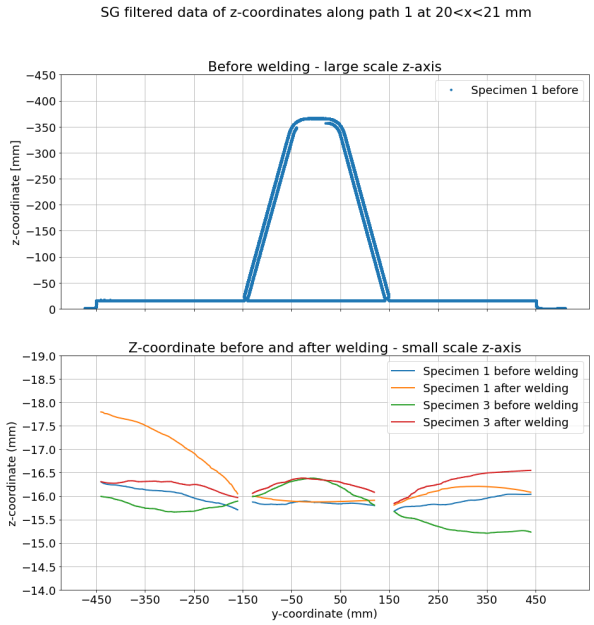

Figure 16. Z-coordinates of top of deck plate along path 1

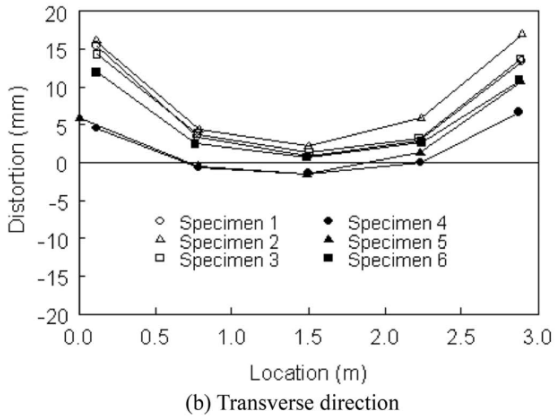

Figure 17. Transverse displacement rib-deck specimens by Sim et al. [1]

3.3 Discussion

The Artec Leo scanner can reach a 3D point accuracy of up to 0.1mm, according to the manufacturer [15]. Settings such as HD density will affect the accuracy. The exact accuracy with the current settings is unknown and needs to be studied in more detail. A scatter of z-coordinates along each path is found. The spread is approximately 0.25mm. The data has been filtered with the SG algorithm. The parameters of this algorithm will affect the accuracy. More advanced scanners need to be used to compare the scattering of the measurements and determine the accuracy. Finally, inaccuracies may occur due to errors occurring during scanning, such as frame misalignments and surface reflections.

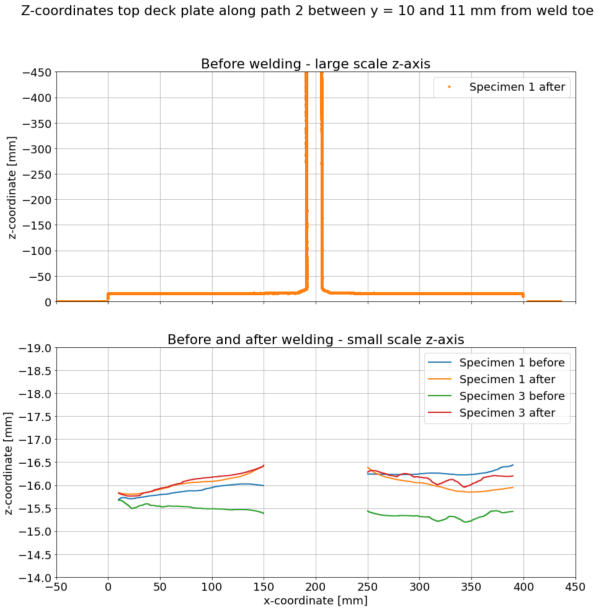

Figure 18. Z-coordinates of top of deck plate along path 2

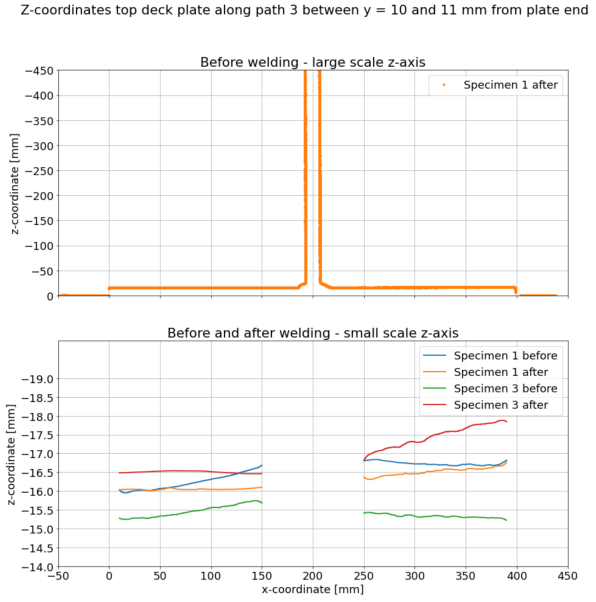

Figure 19. Z-coordinates of top of deck plate along path 3

4 Conclusions

Experimental investigations of deformations and temperature distribution due to welding were performed on the full-scale segment of an OSD. These data are required to optimise welding

procedure, limit distortions and improve the understanding of residual stress state in welded details derived from the deformation field. A new distortion measurement methodology has been established using an advanced handheld 3D scanner. The following conclusions can be drawn from the research.

1. A maximum temperature of 1042 °C 1.8s after welding was recorded.
2. The temperature behind the heat source reduces to 200 °C at 150mm from the heat source. In front and perpendicular to the heat source, the temperature decreases to room temperature at 50 and 150mm, from the heat source, respectively.
3. The maximum measured upward displacement of the 900x400 deck plate was 1.32 mm.
4. The order of magnitude of the deformation is comparable to research by Sim et al. [1]. However, no crossbeam was used in that research. In addition, a different welding procedure and material properties were used, so no strict comparison is justified.
5. The maximum scatter along a path in vertical coordinates was approximately 0.25mm.
6. The established methodology with the 3D scanner is an easy to use and accurate tool for measuring displacements, but scanning must be done carefully to prevent misalignment of frames.

In future work, the obtained data can be compared to data obtained from alternative scanners, such as the Artec spider, or from laser- or 3D photography tracking equipment. The presented data will be used to improve numerical prediction models for simulation of the fatigue lifetime. The accuracy of the chosen boundary conditions in simulating a bridge deck should be investigated by measuring distortions in a full-scale bridge deck. Such findings could help reduce the size of numerical models for predicting the fatigue life of a full-scale bridge deck.

5 References

[1] Sim HB, Uang CM, Sikorsky C. Effects of Fabrication Procedures on Fatigue Resistance of Welded Joints in Steel Orthotropic Decks. *Journal of Bridge Engineering.* 2009 Sep;**14**(5):366-73.

[2] Deng D, Murakawa H, Liang W. Numerical simulation of welding distortion in large structures. *Computer Methods in Applied Mechanics and Engineering.* 2007;**196**(45):4613-27.

[3] Ji B, Liu R, Chen C, Maeno H, Chen X. Evaluation on root-deck fatigue of orthotropic steel bridge deck. *Journal of Constructional Steel Research.* 2013 Nov;**90**:174-83.

[4] de Jong FBP. Overview Fatigue Phenomenon in Orthotropic Bridge Decks in the Netherlands. Sacramento, CA; 2004.

[5] Xin H, Veljkovic M. Effects of residual stresses on fatigue crack initiation of butt-welded plates made of high strength steel; 2019.

[6] Maddox SJ. *Fatigue strength of welded structures.* Cambridge, England: Abington Pub; 1991.

[7] Puymbroeck EV, Staen GV, Iqbal N, Backer HD. Residual weld stresses in stiffener-to-deck plate weld of an orthotropic steel deck. *Journal of Constructional Steel Research.* 2019 Aug;**159**:534-47.

[8] Webster GA, Ezeilo AN. Residual stress distributions and their influence on fatigue lifetimes. *International Journal of Fatigue.* 2001;**23**:375-83.

[9] van Puymbroeck E, Nagy W, De Backer H. Use of the hole drilling method to determine residual weld stresses in bridge constructions; 2016. p. 1-6

[10] Gu Y, Li Y, Zhou Z, Ren S, Kong C. Numerical Simulation and Measurement of Welding Residual Stresses in Orthotropic Steel Decks Stiffened with U-Shaped Ribs. *International Journal of Steel Structures.* 2020 Mar;**20**(3):856-69.

[11] Goldak J, Chakravarti A, Bibby M. A new finite element model for welding heat sources. *Metallurgical Transactions B.* 1984 Jun;**15**(2):299-305.

[12] Manai A, von Bock und Polach RUF, Al-Emrani M. A probabilistic study of welding residual stresses distribution and their contribution to the fatigue life. *Engineering Failure Analysis*. 2020 Dec;**118**:104787.

[13]Karlsson A, Wesley C. Fatigue Analysis for Orthotropic Steel Deck Bridges. Goteborg, Sweden: Chalmers University of Technology; 2015.
[14]Advanced Thermal Imaging Camera FLIR E96;. Accessed: 2022-03-13. https://www.flir.com/products/e96/
[15]Artec-group. Artec Studio 16 User Guide;.

6 Appendix

The data points before filtering of path 1, 2 and 3 are shown in Figure 21,22 and 23, respectively.

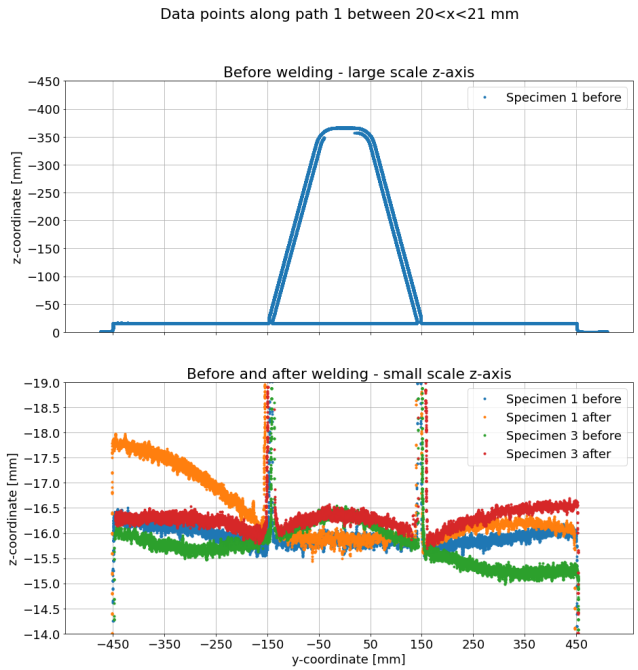

Figure 20. Raw data points along path 1

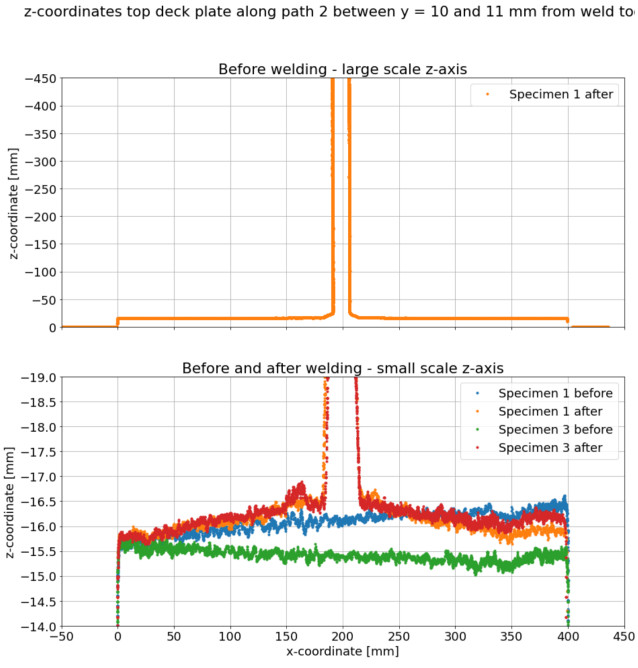

Figure 21. Raw data points along path 2

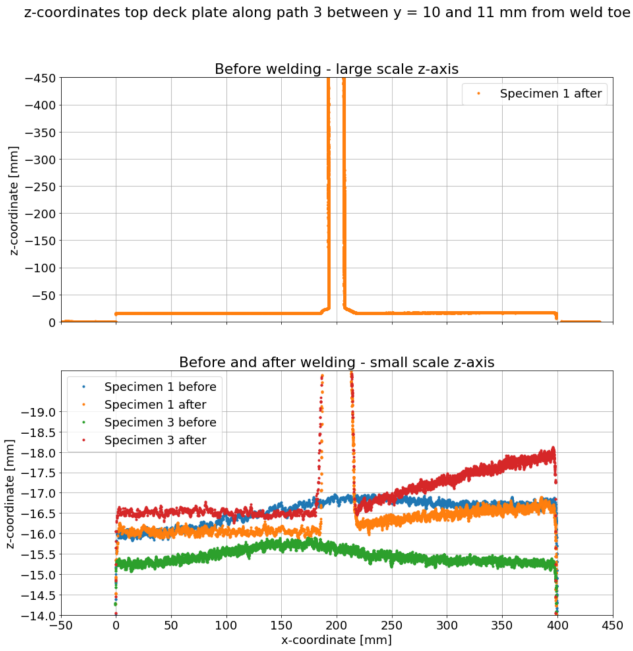

Figure 22. Raw data points along path 3